


Simultaneous *In Situ* Analysis of Carbon and Nitrogen Isotope Ratios in Organic Matter by Secondary Ion Mass Spectrometry

Akizumi Ishida (1, 2, 5)* , Kouki Kitajima (1, 2), Kenneth H. Williford (3), Michael L. Tuite (3), Takeshi Kakegawa (4) and John W. Valley (1, 2)

(1) Department of Geoscience, NASA Astrobiology Institute, University of Wisconsin-Madison, Madison, WI, 53706, USA

(2) Department of Geoscience, WiscSIMS, University of Wisconsin-Madison, Madison, WI, 53706, USA

(3) Jet Propulsion Laboratory, California Institute of Technology, Pasadena, CA, 91109, USA

(4) Department of Earth Science, Graduate School of Science, Tohoku University, Sendai, 9808578, Japan

(5) Present address: Institute for Excellence in Higher Education, Tohoku University, Sendai, 9808576, Japan

* Corresponding author. e-mail: ishidaz@tohoku.ac.jp

An *in situ* measurement method for simultaneous determination of carbon and nitrogen isotope ratios in organic matter was developed by secondary ion mass spectrometry with a spatial resolution of $\sim 12 \mu\text{m}$. Secondary ion intensities of $^{12}\text{C}_2^-$, $^{12}\text{C}^{13}\text{C}^-$, $^{12}\text{C}^{14}\text{N}^-$ and $^{12}\text{C}^{15}\text{N}^-$ were simultaneously measured by three Faraday cups and one electron multiplier. Ions of $^{12}\text{C}_2\text{H}^-$ were measured to monitor hydride interferences and to correct for mass bias. The analytical precisions of $\delta^{13}\text{C}$ and $\delta^{15}\text{N}$ values of a reference material (UWLA-1 anthracite) were 0.16‰ and 0.56‰, respectively (2s). A negative correlation was observed between the mass bias of carbon and $^{12}\text{C}_2\text{H}^-/^{12}\text{C}_2^-$ ratios of examined reference materials. In contrast, there was no correlation between mass bias and hydrogen concentration for nitrogen. The $\delta^{13}\text{C}_{\text{VPDB}}$ and $\delta^{15}\text{N}_{\text{Air}}$ values of twenty-two individual globules of organic matter, found in carbonate rock of the 1878 Ma Gunflint Formation, were determined by the new procedure, ranging from -33.8‰ to -33.3‰ and +4.2‰ to 5.8‰, respectively. Means of $\delta^{13}\text{C}_{\text{VPDB}}$ and $\delta^{15}\text{N}_{\text{Air}}$ values, $-33.5 \pm 0.25\text{‰}$ and $+5.2 \pm 0.81\text{‰}$, are consistent with reported values from bulk sample analysis within analytical precision.

Keywords: secondary ion mass spectrometry, nitrogen isotope ratio, carbon isotope ratio, organic matter, anthracite, Palaeoproterozoic.

Received 01 Sep 17 – Accepted 05 Feb 18

Carbon and nitrogen isotope ratios ($\delta^{13}\text{C}$ and $\delta^{15}\text{N}$) of Precambrian organic matter (OM) have been recognised as key proxies to constrain the evolution of life and transition of redox status of the ocean through geological time (e.g., Schidlowski 1988, Beaumont and Robert 1999, Sigman *et al.* 2009, Thomazo *et al.* 2009). Typically, OM (kerogen or pyrobitumen) was concentrated from bulk samples by hydrochloric and hydrofluoric acid treatments or extracted by organic solvents (bitumen). Nitrogen can be present in OM or as ammonium in phyllosilicates (e.g., Ader *et al.* 2006, Pinti and Hashizume 2011, Stüeken *et al.* 2015). Recent studies suggest that the isotope ratio of nitrogen in kerogen can be altered during metamorphism (e.g., Schimmelmann and Lis 2010, Stüeken *et al.* 2015, 2017). In addition, extraction of kerogen requires a large amount of sample, homogenises multiple reservoirs and any zoning and destroys evidence for complex origins of kerogen in

sedimentary rocks. Although the bulk methods of extraction and analysis allow the fluctuation of isotope ratios of OM to be studied at the centimetre-to-millimetre scale, occurrences of OM at the micrometre scale (such as laminated kerogen or microfossils), minerals, and coexisting relations in micrometre-scale observations yield more detailed records. This high-spatial resolution analysis is beneficial for the comprehensive understanding of the sedimentary environment.

Recently, studies using secondary ion mass spectrometry (SIMS) have targeted OM at the micrometre scale. Such *in situ* analyses of microfossils and minerals in sedimentary rocks reveal new insights into ancient life and the corresponding surface environment of Precambrian Earth (e.g., House *et al.* 2000, Wacey *et al.* 2013, 2016, Williford *et al.* 2013, 2016, Ushikubo *et al.* 2014, Morag *et al.* 2016). During SIMS analysis, carbon is typically ionised as a

monomer ($^{12}\text{C}^-$, $^{13}\text{C}^-$) or dimer ($^{12}\text{C}_2^-$, $^{12}\text{C}^{13}\text{C}^-$, $^{13}\text{C}_2^-$) of negative ions with a positive primary beam ($^{133}\text{Cs}^+$). The high ionisation efficiency of carbon enables a high spatial resolution of elemental mapping and/or isotope ratio determination, targeting carbon-bearing microstructures and biogenic/abiogenic carbonate minerals (e.g., House *et al.* 2000, Williford *et al.* 2013, 2016, Bell *et al.* 2015). Nitrogen, on the other hand, is not efficiently ionised as a monomer negative ion, but is usually ionised as a CN^- molecular ion for SIMS analysis. A few recent studies have measured CN^- ion beam intensities by high-lateral resolution SIMS (NanoSIMS) in a variety of research fields, as indicators of nutrient distributions in the microstructure of foraminifera, heterogeneous isotope distributions of OM in meteorite and diamonds, and a biosignature for putative microfossils (e.g., Wacey *et al.* 2013, 2016, Ito *et al.* 2014, Nomaki *et al.* 2016, Smart *et al.* 2016). In these studies, because the nitrogen concentrations and isotope ratios of examined materials were significantly higher than those of their matrix, only a mapping analysis of relative abundance of nitrogen isotopes was required. For many astrobiology studies, on the other hand, both high-spatial resolution and high-precision (< 1 per mil) measurement methods for isotope ratios are required to reconstruct the palaeo-environment and microbial activity, targeting micrometre-scale OM, *in situ* from sedimentary rocks.

Accurate SIMS measurement results require matrix-matched OM reference materials (RMs) for $\delta^{13}\text{C}$ and $\delta^{15}\text{N}$ values at the nanogram scale. Anthracite can be a suitable RM for the SIMS analysis of OM; it typically consists of 80% to 90% carbon with minor mass fractions of nitrogen, hydrogen, oxygen and sulfur. Williford *et al.* (2016) reported measurement results with precision of $\pm 0.3\text{‰}$ (2s) for $\delta^{13}\text{C}$ values among a series of anthracite RMs by SIMS ^{12}C and ^{13}C ion beam measurement, which is considered to demonstrate no influence of inhomogeneity on the precision. High-precision isotope determinations of $\delta^{13}\text{C}$ and $\delta^{15}\text{N}$ values in diamond were reported by Smart *et al.* (2016) also using an IMS 1280 instrument. They measured ^{12}C and ^{13}C ion beams for the carbon isotope ratio measurements, and $^{12}\text{C}^{14}\text{N}^-$ and $^{12}\text{C}^{15}\text{N}^-$ ions for nitrogen isotope ratio measurements. However, their method needs two separate measurements on different spots and different days because these ions cannot be measured simultaneously.

The purposes of this study were (a) to develop new geometry and aperture settings to measure C and N isotope ratios simultaneously, with high precision and high spatial resolution, (b) to evaluate homogeneity of $\delta^{15}\text{N}$ values in the candidate RM with homogeneous $\delta^{13}\text{C}$ values and (c) to

apply the new method to compare Palaeoproterozoic OM found in carbonate rock from the Gunflint Formation, anthracite from the Michigamme Formation and shungite from the Karelia region of Russia.

Experimental

Potential RM for $\delta^{15}\text{N}$ measurements

Five anthracites, UWLA-1 (LCNN anthracite), UWHA-1 (Harmony anthracite), UWJA-1 (Jeddo anthracite), UWMA-1 (Michigamme anthracite) and PSOC1468 (anthracite, Penn. State Coal std.), and one shungite (SH95-S1a) were selected to evaluate the homogeneity of nitrogen isotope ratios for use as RMs. Approximately 500 μm diameter fragments of each were cast together in the same 25 mm epoxy mount. Their bulk $\delta^{13}\text{C}$ values are reported by Williford *et al.* (2016) (Table 1).

Precambrian organic matter sample

Carbonate rock, with minor detrital quartz grains and globules of organic matter (OM) among a matrix of carbonate minerals, was selected from the Gunflint Formation (1878 Ma; Fralick *et al.* 2002), Ontario, Canada (Figure 1). The $\delta^{13}\text{C}_{\text{VPDB}}$ (defined as $\{R(^{13}\text{C}/^{12}\text{C})_{\text{sample}}/R(^{13}\text{C}/^{12}\text{C})_{\text{VPDB}} - 1\} \cdot 1000$, in per mil notation, where $R(^{13}\text{C}/^{12}\text{C})_{\text{sample}}$ and $R(^{13}\text{C}/^{12}\text{C})_{\text{VPDB}}$ indicate the isotope ratios of carbon for sample and international measurement standard) and $\delta^{15}\text{N}_{\text{Air}}$ (defined as $\{R(^{15}\text{N}/^{14}\text{N})_{\text{sample}}/R(^{15}\text{N}/^{14}\text{N})_{\text{Air}} - 1\} \cdot 1000$, in per mil notation, where $R(^{15}\text{N}/^{14}\text{N})_{\text{sample}}$ and $R(^{15}\text{N}/^{14}\text{N})_{\text{Air}}$ indicate the isotope ratios of nitrogen for sample and international measurement standard) values of this bulk kerogen were obtained by previous studies (sample #0708 in Ishida *et al.* 2012, 2017) and are summarised in Table 1. Sample #0708 was prepared as a 25 mm round thin section with a thickness of approximately 50 μm . Mineralogical observation was carried out by a petrographic and scanning electron microscope with an energy dispersive X-ray spectrometer (SEM/EDS: Hitachi S-3400N). Backscattered electron (BSE) mode was used to investigate the relative chemical heterogeneity in the matrix minerals and examined RMs and samples. OM was observed within ferro-dolomite associated with minor detrital quartz grains, clay minerals and inter-filling calcite (Figure 1). Matrix minerals are reworked carbonate, suggesting the OM has also lost its primary sedimentary structure, and would have migrated between ferro-dolomite grains. OM exists as up to 50 μm globules. Two of the five RMs, UWMA-1 (anthracite from the 1850 Ma Michigamme Formation, Michigan, USA; Tyler *et al.* 1957) and SH95-S1a shungite (2100–2000 Ma Karelia, Russia; Buseck *et al.* 1997), were also investigated to constrain the isotope

Table 1.

Isotope ratios of carbon and nitrogen of reference materials and Gunflint organic matter measured in bulk samples by conventional extraction and gas-source mass spectrometry

RM	Names	C (g/100 g)	N (g/100 g)	$\delta^{13}\text{C}_{\text{VPDB}}$ (‰)	2s (‰)	$\delta^{15}\text{N}_{\text{Air}}$ (‰)	2s (‰)
UWLA-1 ^a	LCNN anthracite	95.7 ^a	1.2 ^a	-23.56 ^a	0.4	5.7	0.5
UWMA-1 ^a	Michigamme anthracite	94.1 ^a	1.2 ^a	-30.75 ^a	0.4	5.0	0.5
UWJA-1 ^a	Jeddo anthracite	95.2 ^a	1.1 ^a	-23.40 ^a	0.4	3.3	1.4
UWHA-1 ^a	Harmony anthracite	94.0 ^a	1.0 ^a	-22.62 ^a	0.2	5.1	0.5
PSOC1468 ^a	Anthracite, Back Mt. seam	89.0 ^a	0.8 ^a	-23.52 ^a	0.6	4.9	0.5
SH95-S1 ^a	Karelia shungite	66.0 ^a	0.8	-37.12 ^a	0.3	2.9	1.0
Kerogen (Gunflint carbonate (#0708)) ^b		84.6	0.2	-32.9	0.4	6.9	0.6

^a $\delta^{13}\text{C}$ values of anthracites and shungite were from Williford *et al.* (2016).

^b Bulk data of Gunflint kerogen (#0708) were from Ishida *et al.* (2012, 2017).

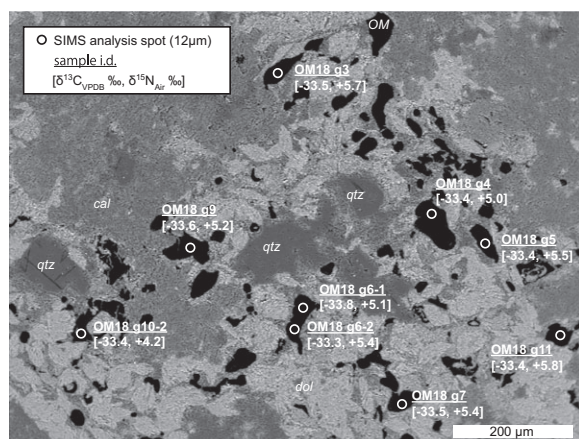


Figure 1. BSE image of carbonate thin section #0708 from the Gunflint Formation. Organic matter forms globules (OM) among ferro-dolomite matrix (Dol) with diameter of ~ 50 μm. Matrix consists of ferro-dolomite, and in-filling calcite (Cal) with detrital quartz grains (Qtz) and minor clay minerals. SIMS spots in OM (circles) are labelled with $\delta^{13}\text{C}_{\text{VPDB}}$ and $\delta^{15}\text{N}_{\text{Air}}$ values ([$\delta^{13}\text{C}_{\text{VPDB}}$, $\delta^{15}\text{N}_{\text{Air}}$]).

distribution of carbon and nitrogen in Palaeoproterozoic sedimentary rocks.

Bulk nitrogen isotope ratio measurement results of RMs

The $\delta^{15}\text{N}$ values of bulk aliquots of each potential RM were determined by gas-source isotope ratio mass spectrometry. Unweathered and cleaned rock fragments, which were prepared from the same portion with the mounted RMs, were finely powdered using an agate

mortar. Measurements were performed by an elemental analyser connected to an isotope ratio mass spectrometer housed in the Astrobiogeochemistry Laboratory (abclab) at the Jet Propulsion Laboratory, USA (Costech 4010 and Delta V Plus), and Tohoku University, Japan (Flash2000 and Delta V Advantage). An approximately 5 mg test portion of powder was used for each measurement. Typical repeatability precision of $\pm 0.5\text{‰}$ (2s, standard deviations) was determined by repeat measurements of isotopic reference materials in both instruments. The precision of bulk $\delta^{15}\text{N}$ values for each RM is shown in Table 1 (quoted as 2s). Unless otherwise noted, the '2s' represents standard deviation, not standard error hereafter in this study.

Secondary ion mass spectrometry instrumentation

Carbon and nitrogen isotope measurements were conducted using a CAMECA IMS 1280, a large-radius multi-collector ion microprobe, housed at the WiscSIMS Laboratory, University of Wisconsin-Madison. Two sessions were performed: session 1 (17 February–19 February 2016) was to evaluate homogeneity of $\delta^{15}\text{N}$ values of RMs, and session 2 (11 July–13 July 2016) was conducted to develop the simultaneous carbon and nitrogen isotope measurement method and to apply it to Palaeoproterozoic OM. In general, we followed the basic measurement procedure of SIMS described in previous studies (e.g., Kita *et al.* 2009, Valley and Kita 2009, Ushikubo *et al.* 2014, Williford *et al.* 2016). Sample mounts were degassed for more than 24 hr to below 1.33×10^{-5} Pa in the storage chamber of the SIMS. In both sessions, a primary $^{133}\text{Cs}^+$ beam with an intensity of 2.5 nA and total impact energy of 20 keV was focused on the sample surface with a spot diameter of ~ 12 μm. The secondary optics were configured as follows: transfer lens magnification of 200, contrast aperture diameter

of 400 μm , field aperture of 4000 $\mu\text{m} \times 4000 \mu\text{m}$, entrance slit width of 30 μm , and energy slit width of 40 eV. An electron gun and gold coating (up to 25 nm of thickness) on the sample surface were used to provide charge compensation. The total measurement time was ~ 300 s (5 min) for one spot consisting of 60 s for pre-sputtering, 60 s to centre the secondary ion beam (DTFA-X, DTFA-Y) and 160 s (8 s \times twenty cycles) of measurement time. The baseline intensities of Faraday cup detectors (FCs) were determined before the beginning of each day's measurement. The dead time of the electron multiplier (EM, 68 ns) was also corrected. After SIMS measurements, all pits were imaged and analysed by SEM/EDS.

Session 1: homogeneity of $\delta^{15}\text{N}$ in potential RMs

The homogeneity of nitrogen isotope ratios of each RM was examined in session 1. Secondary molecular ions of $^{12}\text{C}^{14}\text{N}^-$ and $^{12}\text{C}^{15}\text{N}^-$ were collected simultaneously using the combination of Faraday cup (FC) detector with $10^{10} \Omega$ resistor on the L'2 position and electron multiplier (EM) detector on the axial position. Mass-resolving power (MRP) of ~ 8000 was achieved with aperture settings of 30 μm for the entrance slit and 150 μm for the exit slit for both FC and EM. Measured nitrogen isotope ratios ($\delta^{15}\text{N}_{\text{meas}}$) are expressed in per mil notation (‰) as follows:

$$\delta^{15}\text{N}_{\text{meas}} = 1000 \times \left[\frac{(^{12}\text{C}^{15}\text{N}^- / ^{12}\text{C}^{14}\text{N}^-)_{\text{measured}}}{(^{15}\text{N}/^{14}\text{N})_{\text{Air}}} - 1 \right] \quad (1)$$

where $(^{12}\text{C}^{15}\text{N}^- / ^{12}\text{C}^{14}\text{N}^-)_{\text{measured}}$ denotes a ratio of measured count rates of $^{12}\text{C}^{15}\text{N}^-$ and $^{12}\text{C}^{14}\text{N}^-$ ions and $(^{15}\text{N}/^{14}\text{N})_{\text{Air}}$ is 0.0036765 (Junk and Svec 1958). The precise correction of peak intensity and mass bias calibration were omitted during the session 1, because the aim of this session was to determine the heterogeneity of each RM.

Session 2: development of simultaneous measurement of $\delta^{13}\text{C}$ and $\delta^{15}\text{N}$

To achieve simultaneous measurement of carbon and nitrogen isotope ratios, we measured four molecular ions simultaneously ($^{12}\text{C}_2^-$, $^{12}\text{C}^{13}\text{C}^-$, $^{12}\text{C}^{14}\text{N}^-$ and $^{12}\text{C}^{15}\text{N}^-$). The detector geometry and aperture settings are shown in Figure 2. Secondary ions were collected by Faraday cup (FC) detectors on the positions of L'2 with a $10^{10} \Omega$ resistor, C and H1 with $10^{11} \Omega$ resistors and with an electron multiplier (EM) on H2 (low to high mass, respectively). The $^{12}\text{C}_2\text{H}^-$ ion was automatically measured by peak jumping on the FC on C position at the end of each measurement by changing the voltage of DSP2X deflectors after the magnetic field. During RM measurements, count rates of $^{12}\text{C}^{14}\text{NH}^-$

were also checked manually after each measurement using the FC in the C position to test for a correlation with the count rates of $^{12}\text{C}_2\text{H}^-$ ion (see Mass bias calibration in Results and discussion).

The exit slit configuration was modified for this session. These slits are located immediately before the ion detectors and can be changed to adjust mass-resolving power. The standard configuration of an IMS 1280 has three different exit slit widths that must be set to be the same for each movable detector: 500, 250 or 150 μm corresponding to the slit positions of #1, #2 and #3, respectively. Different slit widths can be manufactured for specific purposes. Ushikubo *et al.* (2014) modified slits in position #2 to optimise MRP for simultaneous detection of four sulfur isotopes using four FCs. In the present study, slit position #3 was modified as follows: 150 μm width for the FCs on C and H1 positions and the EM on H2, while 500 μm width was used for the FC on L'2 position, resulting in MRP of ~ 8000 for FCs on C and H1, and EM, and of ~ 2000 for FC on L'2 (Appendix S1). High MRP is required on C, H1 and H2 positions to separate isobaric interferences. The wider exit slit was applied for L'2 because it was placed further from the optic axis to detect $^{12}\text{C}_2^-$ ions. Other secondary optics were configured as for session 1. The detector positions and slit settings described above improved the count rate and stability of secondary ions during measurement.

Tailing interference

Tailing interferences from adjacent peaks were calculated on each mass according to the procedure described by Kita *et al.* (2009) and Ushikubo *et al.* (2014). Typical count rates described in the following paragraph were obtained from UWLA-1 anthracite in session 2. Although the actual source of these divergent ions that made a tailing interference was unclear in this study, the effect can be estimated and be corrected by the following procedure. The $^{12}\text{C}_2^-$ ion (L'2) does not have neighbouring peaks that make a tailing interference. The $^{12}\text{C}^{13}\text{C}^-$ ion (C) is near the peak of $^{12}\text{C}_2\text{H}^-$ and was separated at $\text{MRP} = 5600$. The typical count rate on anthracite was 1.8×10^7 counts per second (cps) for $^{12}\text{C}^{13}\text{C}^-$ and 1.8×10^8 cps for $^{12}\text{C}_2\text{H}^-$. The contribution of $^{12}\text{C}_2\text{H}^-$ tailing interference ($^{12}\text{C}_2\text{H}_{\text{tail}}^-$) to the $^{12}\text{C}^{13}\text{C}^-$ was estimated by the following steps: (a) calculation of the mass difference between $^{12}\text{C}_2\text{H}^-$ and $^{12}\text{C}^{13}\text{C}^-$ (0.00447 Da), (b) measurement of the intensity of $^{12}\text{C}^{13}\text{C}^-$ mass spectrum at 0.00447 Da below the $^{12}\text{C}^{13}\text{C}^-$ peak centre and (c) calculation of the relative intensity factor of $^{12}\text{C}^{13}\text{C}^-$ ($\text{RIF}_C = ^{12}\text{C}^{13}\text{C}_{\text{tail}}^- / ^{12}\text{C}^{13}\text{C}_{\text{peak}}^-$) and (d) of the $^{12}\text{C}_2\text{H}_{\text{tail}}^-$, which was calculated by the RIF_C and measured count rate of $^{12}\text{C}_2\text{H}^-$. We assumed that the mass spectrum shapes of

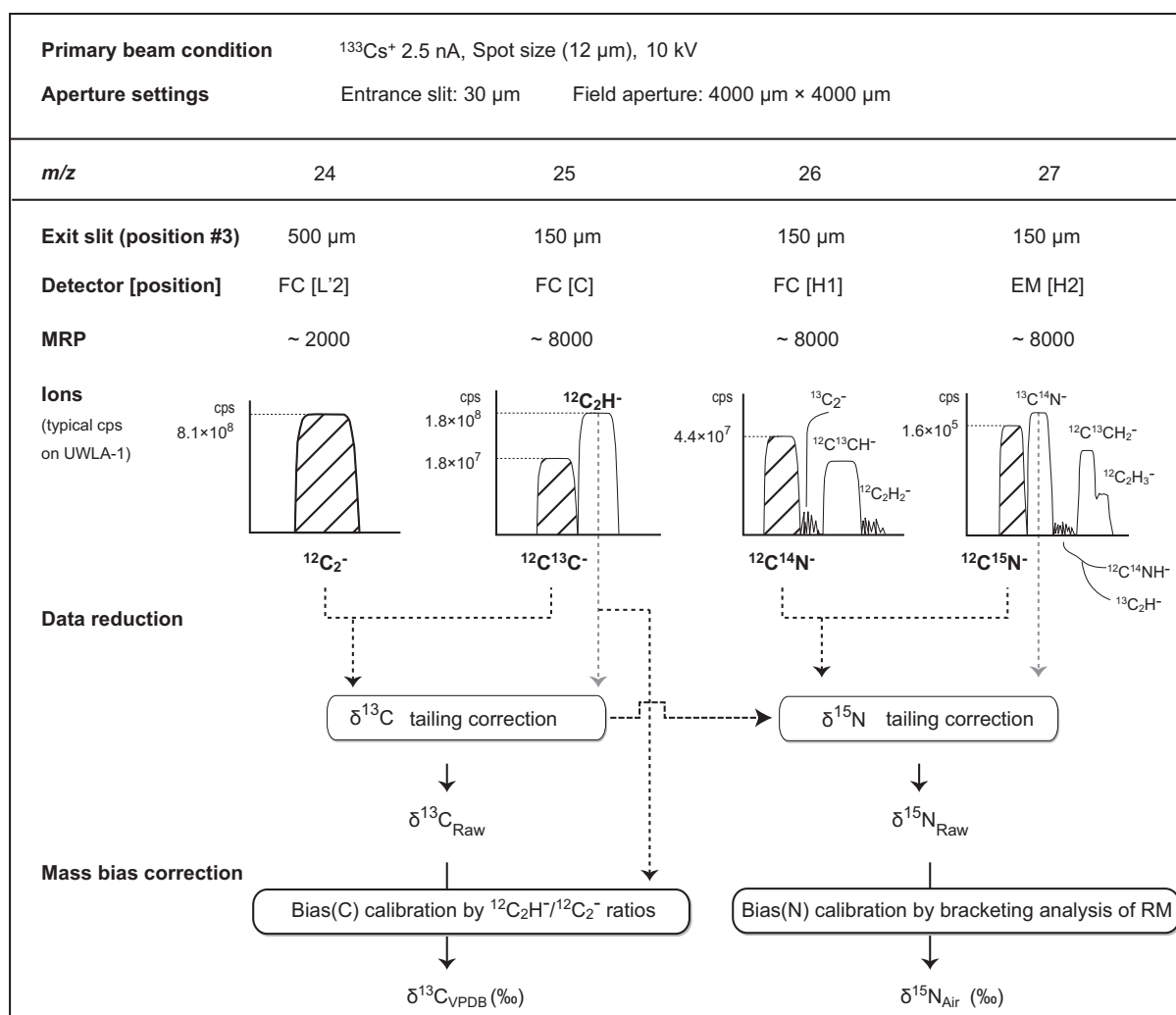


Figure 2. Chart of measurement conditions developed for simultaneous measurement of $\delta^{13}\text{C}$ and $\delta^{15}\text{N}$. Four detectors were used to measure molecular ion beam intensities. Mass spectrometer exit slits (at entrance of detectors) were modified to attain different mass-resolving power (MRP) on each detector to separate isobaric interferences while optimising intensity. Tailing from adjacent peaks on $^{12}\text{C}^{13}\text{C}^-$ and $^{12}\text{C}^{15}\text{N}^-$ ions was measured and subtracted from main peaks. After the tailing corrections, both $\delta^{13}\text{C}_{\text{VPDB}}$ and $\delta^{15}\text{N}_{\text{Air}}$ values were obtained by the mass bias calibrations defined by reference material measurements in session 2.

$^{12}\text{C}^{13}\text{C}^-$ and $^{12}\text{C}_2\text{H}^-$ were the same because the direct ion images of these two ions were very similar. The RIF_{C} in session 2 was calculated as 6.0×10^{-5} . Then, the $^{12}\text{C}_2\text{H}_{\text{tail}}^-$ was calculated as $\sim 1.0 \times 10^4$ cps, corresponding to 0.52‰ of $^{12}\text{C}^{13}\text{C}^-$ counts. These tailing interferences were subtracted from measured values based on the tailing ratio and count rate of $^{12}\text{C}_2\text{H}^-$ in each measurement. Finally, we obtained tailing-corrected $\delta^{13}\text{C}$ values ($\delta^{13}\text{C}_{\text{Raw}}$) defined as follows:

$$\delta^{13}\text{C}_{\text{Raw}} = 1000 \times \left[\frac{(^{13}\text{C}/^{12}\text{C})_{\text{measured}}}{(^{13}\text{C}/^{12}\text{C})_{\text{VPDB}}} - 1 \right] \quad (2)$$

$$(^{13}\text{C}/^{12}\text{C})_{\text{measured}} = 0.5 \times \frac{(^{12}\text{C}^{13}\text{C}^- - ^{12}\text{C}_2\text{H}_{\text{tail}}^-)}{^{12}\text{C}_2^-} \quad (3)$$

$$^{12}\text{C}_2\text{H}_{\text{tail}}^- = \text{RIF}_{\text{C}} \times ^{12}\text{C}_2\text{H}^- \quad (4)$$

where $^{12}\text{C}^{13}\text{C}^-$, $^{12}\text{C}_2^-$ and $^{12}\text{C}_2\text{H}^-$ are measured count rates. The factor of 0.5 was derived by the probability of generating $^{12}\text{C}_2^-$ and $^{12}\text{C}^{13}\text{C}^-$ ions in the combination of ^{12}C and ^{13}C ($^{12}\text{C}_2^-$, $2 \times ^{12}\text{C}^{13}\text{C}^-$ and $^{13}\text{C}_2^-$ can be generated). The ratio $(^{13}\text{C}/^{12}\text{C})_{\text{VPDB}}$ is defined as 0.0112372 from $^{13}\text{C}/^{12}\text{C}$ ratio of Pee Dee Belemnite (Craig 1957).

The closest neighbour peak of $^{12}\text{C}^{14}\text{N}^-$ (detector position H1) was $^{13}\text{C}_2^-$ which is resolved at $\text{MRP} = 7200$. The typical count rate of $^{13}\text{C}_2^-$ was $< \sim 10^4$ cps on UWLA-1 anthracite, which was $\sim 10^3$ lower than the count rate of $^{12}\text{C}^{14}\text{N}^-$ (4.4×10^7 cps). Even if we assumed the same tailing factor with $^{12}\text{C}_2\text{H}_{\text{tail}}^- / ^{12}\text{C}_2\text{H}_{\text{peak}}^-$ (6.0×10^{-5}), the tailing of $^{13}\text{C}_2^-$ was calculated as a few cps. Thus, the tailing correction for $^{12}\text{C}^{14}\text{N}^-$ was calculated as less than 0.007‰, which is negligible compared with the counting statistics.

The $^{12}\text{C}^{15}\text{N}^-$ ion (detector position H2) has a neighbouring peak of $^{13}\text{C}^{14}\text{N}^-$ which requires $\text{MRP} = 4300$. The typical count rate of $^{12}\text{C}^{15}\text{N}^-$ was 1.6×10^5 cps for UWLA-1 anthracite. The contribution of $^{13}\text{C}^{14}\text{N}^-$ tailing interference ($^{13}\text{C}^{14}\text{N}_{\text{tail}}^-$) to the $^{12}\text{C}^{15}\text{N}^-$ was estimated by the same procedure used for carbon. The mass difference between $^{12}\text{C}^{15}\text{N}^-$ and $^{13}\text{C}^{14}\text{N}^-$ was calculated as 0.00632 Da. The relative intensity factor of nitrogen (RIF_N) was determined by the relative intensity of $^{12}\text{C}^{15}\text{N}^-$ mass spectrum at 0.00632 Da below the $^{12}\text{C}^{15}\text{N}^-$ peak centre ($\text{RIF}_\text{N} = ^{12}\text{C}^{15}\text{N}_{\text{tail}}^- / ^{12}\text{C}^{15}\text{N}_{\text{peak}}^-$). Then, the $^{13}\text{C}^{14}\text{N}_{\text{tail}}^-$ could be calculated by the RIF_N and the count rate for $^{13}\text{C}^{14}\text{N}^-$. A count rate for $^{13}\text{C}^{14}\text{N}^-$ ions can be calculated from that of the $^{12}\text{C}^{14}\text{N}^-$ and $^{13}\text{C}/^{12}\text{C}$ ratio of each analytical spot. The typical count rate of $^{12}\text{C}^{14}\text{N}^-$ was $\sim 4.4 \times 10^5$ cps, and the RIF_N was $\sim 1.9 \times 10^{-5}$ on the UWLA-1 anthracite. We obtained tailing-corrected $\delta^{15}\text{N}$ value ($\delta^{15}\text{N}_{\text{Raw}}$) defined as follows:

$$\delta^{15}\text{N}_{\text{Raw}} = 1000 \times \left[\frac{(^{12}\text{C}^{15}\text{N}^- - ^{13}\text{C}^{14}\text{N}_{\text{tail}}^-) / ^{12}\text{C}^{14}\text{N}^-}{(^{15}\text{N}/^{14}\text{N})_{\text{Air}}} - 1 \right] \quad (5)$$

$$^{13}\text{C}^{14}\text{N}_{\text{tail}}^- = \text{RIF}_\text{N} \times (^{13}\text{C}/^{12}\text{C})_{\text{measured}} \times ^{12}\text{C}^{14}\text{N}^- \quad (6)$$

The $^{13}\text{C}^{14}\text{N}_{\text{tail}}^-$ was calculated as ~ 10 cps, corresponding to the 0.056‰ in UWLA-1. The magnitude of this tail depends on the $(^{13}\text{C}/^{12}\text{C})_{\text{measured}}$ ratio (calculated by Equation 3) of each measurement spot; thus, the tailing interferences were subtracted from measured $\delta^{15}\text{N}_{\text{Raw}}$ values based on the tailing ratio and count rate of $^{12}\text{C}^{14}\text{N}^-$ and $(^{13}\text{C}/^{12}\text{C})_{\text{measured}}$ ratio on each measurement spot. The simultaneous isotope ratio measurement method of carbon and nitrogen in this study enables precise evaluation of tailing correction of nitrogen, using carbon isotope ratio determined in the same spot (Figure 2).

Results and discussion

Bulk $\delta^{15}\text{N}$ and chemical composition of RMs and Gunflint OM

Measured bulk $\delta^{15}\text{N}_{\text{Air}}$ values of RMs, ranging from +2.9 to +5.7‰, are summarised in Table 1. Mass fractions

of five elements (H, C, N, O and S) in RMs are summarised in Appendix S2 (this study, Ishida *et al.* 2012, Williford *et al.* 2016). The chemical compositions were also measured by SEM/EDS adjacent to the SIMS pits. There was no significant difference in chemical composition or visible mineral inclusions in RM and the Gunflint OM. BSE images of individual SIMS pits in the Gunflint OM are shown in Appendix S3.

Homogeneity and analytical precision of $\delta^{15}\text{N}$ in RMs (session 1)

The homogeneity of nitrogen isotope ratios of RMs was examined in session 1 before starting simultaneous C and N isotope measurement (Table 2; Appendix S4). Measurements were performed with one spot each on five to twelve grains of each of the six RMs. UWLA-1 and UWMA-1 anthracites show better precision of $\delta^{15}\text{N}_{\text{meas}}$ values for each bracket than other anthracites ($\pm 0.36\%$, $n = 62$, and $\pm 0.40\%$, $n = 10$, respectively, 2s). Both RMs are fit for intended purpose to use as a RM during the analysis of OM samples. Taking into consideration the better homogeneity of carbon isotope ratios reported by Williford *et al.* (2016), we used UWLA-1 as a RM for quality control of analysis during OM measurements. SH95-S1a (shungite) shows the most homogeneous $\delta^{15}\text{N}_{\text{meas}}$ values ($\pm 0.21\%$, $n = 8$, 2s); however, shungite was not used as a RM because the carbon mass fractions of UWLA-1 are closer to that of the sample OM from the Gunflint Formation (Appendix S2). No systematic change in $\delta^{15}\text{N}_{\text{meas}}$ values of UWLA-1 was observed during session 1 (Appendix S5). Mass bias of nitrogen between $\delta^{15}\text{N}_{\text{meas}}$ and bulk $\delta^{15}\text{N}_{\text{Air}}$ values ranged from -8.7 to -7.0‰ with a mean of $-8.2 \pm 1.4\%$ (2s) in the examined RMs (Table 2).

Table 2. Summary of nitrogen isotope precision and mass bias for *in situ* SIMS measurements of reference materials in session 1

RM	Grain	Number of analyses	2s (%)	Mass bias of nitrogen ^a (%)
UWLA-1	12	62	0.43	-8.3
UWMA-1	9	10	0.40	-7.7
UWJA-1	5	5	0.78	-8.8
UWHA-1	5	5	2.11	-7.0
PSOC1468	8	9	0.53	-8.7
SH95-S1a	8	8	0.21	-8.4
			Mean	-8.2
			2s	1.4

^a Mass bias of nitrogen in per mil notation ($\delta^{15}\text{N}$).

Orientation effects could be ignored in the present study, because all examined materials are polycrystalline (Kita *et al.* 2011). Two amber samples from Williford *et al.* (2016) (Baltic and Dominican amber) were also studied. However, the ionisation efficiency of CN^- of amber was significantly lower than for anthracite (Appendix S4). This is because the main component of amber is terpenoid, which does not contain nitrogen (Mills *et al.* 1984). Thus, they were not suitable as calibration RMs in the isotope ratio measurements of nitrogen.

Simultaneous measurement of $\delta^{13}C$ and $\delta^{15}N$ (session 2)

In session 2, the newly developed exit slit and detector geometries were applied to detect $^{12}C_2^-$, $^{12}C^{13}C^-$, $^{12}C^{14}N^-$ and $^{12}C^{15}N^-$ ions simultaneously (Figure 2 and Appendix S1). First, we analysed the five anthracite RMs and the shungite RM to examine the intermediate precision of $\delta^{13}C_{Raw}$ and $\delta^{15}N_{Raw}$ measurement results using the new setting. The $^{12}C_2H^-/^{12}C_2^-$ ratios were also measured to evaluate whether correlations exist with mass bias calibrations for carbon and nitrogen isotope ratios. After calibration tests were completed, $\delta^{13}C$ and $\delta^{15}N$ values were measured in OM from Gunflint Formation sedimentary rock using the procedure and mass bias calibration established by the RM analyses in the same session. UWLA-1 was mounted and polished in the thin section and used as a RM for quality control of analysis. To monitor and correct for any possible shift of isotope ratios caused by a subtle change of conditions, bracketing measurements were made of UWLA-1 before and after measurements of 13–18 samples.

Measurement results of the RMs are summarised in Table 3. The ion yields for $^{12}C_2^-$ and $^{12}C^{14}N^-$ of anthracite and shungite RM ranged from 300 to 350×10^6 cps per 1 nA of primary ion beam (Mcps nA^{-1}) and 15 to 23 Mcps nA^{-1} , respectively. Ratios of $^{12}C_2H^-/^{12}C_2^-$ range from 0.07 to 0.27. The 2s precision of UWLA-1 measurement results was 0.16‰ for $\delta^{13}C$ and 0.56‰ for $\delta^{15}N$, respectively ($n = 20$). The analytical precision of carbon isotope ratio measurement results of UWLA-1 was better than reported by Williford *et al.* (2016) using the ^{12}C ion ($\pm 0.34\%$).

Mass bias calibration

For carbon isotope measurement results of OM by SIMS, a negative correlation between the mass bias of carbon isotope ratio and $^{12}CH^-/^{12}C^-$ ratio was reported by Williford *et al.* (2016). To examine this correlation for the conditions of the present study, the mass biases of carbon (Bias(C)) and nitrogen (Bias(N)) were calculated by the following equations:

Table 3. Summary of SIMS measurement results on reference materials in session 2. For full data set, see Appendix S4

Sample ID	N	$\delta^{13}C_{RMS}^a$ (‰)	2s (%)	$\delta^{15}N_{Air}^a$ (‰)	2s (%)	Bias (C) (%)	Bias (N) (%)	$\delta^{13}C_{Raw}$ (‰)	2s (%)	$\delta^{15}N_{Raw}$ (‰)	2s (%)	$^{12}C_2$ (Mcps nA^{-1})	2s (Mcps nA^{-1})	$^{12}C^{14}N$ (Mcps nA^{-1})	2s ($^{12}C^{14}N$) (Mcps nA^{-1})	$^{12}C_2H/^{12}C_2$	2s	$^{12}C_2H$ tail ^c (%)	$^{13}C^{14}N$ tail ^d (%)	$^{12}C^{14}NH/^{12}C^{14}N^e$	
UWLA-1	20	Bracket	0.16	Bracket	0.56	-7.0	-11.6	-30.4	0.16 ^b	-5.95	0.56 ^b	332	7	17.1	2.41E-02	0.20	2.41E-02	0.541	0.056	5.05E-04	
UWMA-1	4	-30.8	0.15	5.9	0.70	-6.3	-10.8	-36.8	0.22	-5.86	0.35	350	9	23.4	5.14E-03	0.11	5.14E-03	0.292	0.056	2.13E-04	
UWJA-1	4	-23.3	0.16	5.0	0.54	-7.5	-10.1	-30.7	0.73	-6.86	1.10	300	77	16.9	2.91E-02	0.22	2.91E-02	0.582	0.056	5.62E-04	
UWHA-1	4	-23.0	0.19	5.1	0.32	-8.8	-11.5	-31.2	0.29	-6.45	0.66	324	59	17.3	4.01E-03	0.27	4.01E-03	0.733	0.056	6.27E-04	
PSOC	4	-23.4	0.16	4.6	0.54	-7.9	-12.0	-31.2	0.74	-7.18	0.45	328	6	14.8	7.97E-03	0.25	7.97E-03	0.665	0.056	6.92E-04	
1468																					
SH95S1a	4	-37.2	0.15	3.1	0.70	-5.8	-11.5	-42.7	1.03	-8.62	0.90	351	2	14.9	4.81E-03	0.07	4.81E-03	0.196	0.055	2.12E-04	

^a Values were calculated using Equations (12, 13), with the bracketing measurements of UWLA-1.

^b 2s of UWLA-1 is the average of four bracketing measurements.

^c Amount of tailing correction (in ‰ notation) for the interference of $^{12}C_2H$ tail signal to the $^{12}C^{13}C$.

^d Amount of tailing correction (in ‰ notation) for the interference of $^{13}C^{14}N$ tail signal to the $^{12}C^{14}N$.

^e $^{12}C^{14}NH$ was measured manually after each RM analysis.

$$\text{Bias (C)} = 1000 \times (\alpha^{13}\text{C}_{\text{SIMS}} - 1) \quad (7)$$

$$\alpha^{13}\text{C}_{\text{SIMS}} = \frac{(1 + (\delta^{13}\text{C}_{\text{Raw}}/1000))}{(1 + (\delta^{13}\text{C}_{\text{VPDB}}/1000))} \quad (8)$$

$$\text{Bias (N)} = 1000 \times (\alpha^{15}\text{N}_{\text{SIMS}} - 1) \quad (9)$$

$$\alpha^{15}\text{N}_{\text{SIMS}} = \frac{(1 + (\delta^{15}\text{N}_{\text{Raw}}/1000))}{(1 + (\delta^{15}\text{N}_{\text{Air}}/1000))} \quad (10)$$

where Bias(C) and Bias(N) are mass biases in ‰ for carbon and nitrogen; $\delta^{13}\text{C}_{\text{Raw}}$ and $\delta^{15}\text{N}_{\text{Raw}}$ are tailing-corrected values (calculated by Equations 2–5); and $\delta^{13}\text{C}_{\text{VPDB}}$ and $\delta^{15}\text{N}_{\text{Air}}$ are isotope values for RMs (relative to VPDB and Air, respectively), which were determined by conventional gas-source mass spectrometry (Table 1). Bias(C) ranged from -8.8 to -5.8‰ and was smaller than values reported by Williford *et al.* (2016) who measured single carbon ions ($^{13}\text{C}^-$, $^{12}\text{C}^-$). A negative correlation between Bias(C) and $^{12}\text{C}_2\text{H}^+ / ^{12}\text{C}_2^-$ ratios was observed for anthracite and shungite measurements (Figure 3a). The linear regression of the trend ($R^2 = 0.94$) between Bias(C) and $^{12}\text{C}_2\text{H}^+ / ^{12}\text{C}_2^-$ is expressed as follows:

$$\text{Bias (C)} = -13.451 \times \frac{^{12}\text{C}_2\text{H}^+}{^{12}\text{C}_2^-} - 4.679 \quad (11)$$

Bias(C) for each measurement spot on OM samples was calculated by Equation (11) and $^{12}\text{C}_2\text{H}^+ / ^{12}\text{C}_2^-$ ratios measured on that spot.

In contrast to carbon, no correlation was observed between Bias(N) and $^{12}\text{C}_2\text{H}^+ / ^{12}\text{C}_2^-$ ratios (Figure 3b). Bias (N) was essentially constant with mean value of $-11.25 \pm 1.35\%$ (2s, range = -12.0 to -10.1‰). The mass biases of nitrogen on RMs were not the same as those of session 1, because the detector configurations and geometries were completely different between the sessions. The 2‰ difference in the mass bias between examined RMs is caused by UWJA-1, which has 1.4‰ precision in the bulk $\delta^{15}\text{N}$ measurements (Table 1). UWJA-1 might have heterogeneously distributed components with significantly different $\delta^{15}\text{N}$, indicating that this is not suitable as a calibration RM for $\delta^{15}\text{N}$ analysis. This is the first report of SIMS measurements that tested for a correlation between the magnitude of Bias(N) and hydrogen concentrations ($^{12}\text{C}_2\text{H}^+ / ^{12}\text{C}_2^-$) in OM. Considering the strong correlation of mass bias for carbon isotope ratio during SIMS analyses, hydrogen concentrations should be considered with the generation of secondary ions for N and other elements; the lack of a correlation seen here may not apply under different measurement conditions. Hydride ions, such as $^{12}\text{C}_2\text{H}^-$, can be used for monitoring bias of carbon; however, in our analytical procedure,

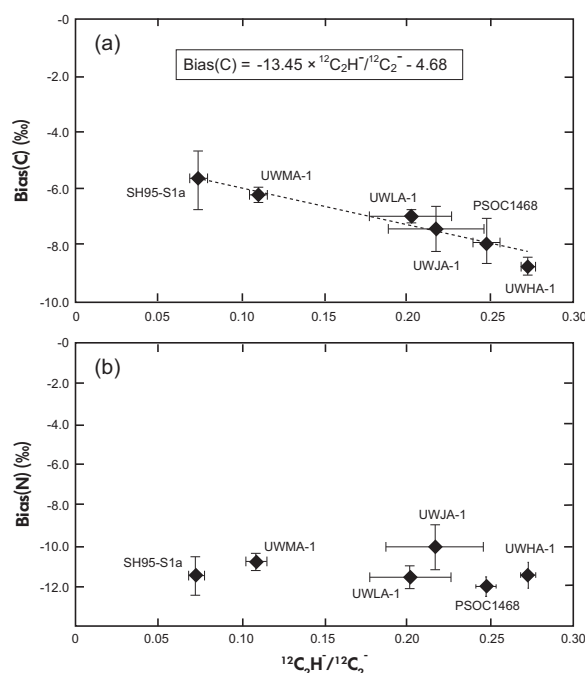


Figure 3. Correlation of SIMS analytical mass bias for (a) carbon and (b) nitrogen isotope ratios against $^{12}\text{C}_2\text{H}^+ / ^{12}\text{C}_2^-$ ratios, measured on five anthracite reference materials and one shungite reference material in session 2.

$^{12}\text{C}^{14}\text{NH}^-$ could not be measured simultaneously during sample OM measurements because $^{12}\text{C}^{15}\text{N}^-$ (also at $\sim m/z = 27$) was measured. Instead, count rates of $^{12}\text{C}^{14}\text{NH}^-$ ions were measured manually on each RM at the end of every measurement to determine the $^{12}\text{C}^{14}\text{NH}^- / ^{12}\text{C}^{14}\text{N}^-$ ratios (Table 3). This procedure added 60 s to the time for each run. Appendix S6a shows the positive correlation between $^{12}\text{C}_2\text{H}^+ / ^{12}\text{C}_2^-$ ratios and $^{12}\text{C}^{14}\text{NH}^- / ^{12}\text{C}^{14}\text{N}^-$ ratios of RMs, suggesting $^{12}\text{C}_2\text{H}^+$ can be used as a measure of hydrogen content as a proxy for $^{12}\text{C}^{14}\text{NH}^-$. Sangely *et al.* (2005) suggested that the relationship between mass bias of carbon and hydrogen concentrations could be explained by the secondary collision of molecular ions on the sample surface caused by the implantation of ions from the primary Cs^+ beam. They preferred this interpretation rather than differences of chemical bonding and vibrational frequency because graphite, which has strong double bonds of carbon, should have the strongest isotope fractionation when ionised, suggesting that a larger mass bias should be observed in samples which have low H/C ratios (i.e., highly graphitised). However, this model cannot explain the absence of correlation between Bias(N) and $^{12}\text{C}_2\text{H}^+ / ^{12}\text{C}_2^-$ ratios (Figure 3b). In addition, the $^{12}\text{C}_2^-$ yields do not correlate with

both Bias(N) and $^{12}\text{C}^{14}\text{N}^-$ yields, suggesting that the difference of graphitisation does not appear to affect the mass bias factor of nitrogen (Appendix S6b–d). Thus, in the present study, mass bias of nitrogen for each measurement of an unknown sample was determined by the average of bracketing measurements of UWLA-1, without a correction for $^{12}\text{C}_2\text{H}^+/^{12}\text{C}_2^-$ ratio.

Data threshold and evaluation of contamination for OM sample analysis

In the present study, data of OM samples were examined by SEM/EDS for evidence of contamination by inclusions of other phases. Spot measurements were considered suspect if the intensity of $^{12}\text{C}_2^-$ or the ratios of $^{12}\text{C}_2\text{H}^+/^{12}\text{C}_2^-$ are out of the range of RM measurements summarised in Table 3. Threshold values for OM sample analysis were set if the yield of $^{12}\text{C}_2^-$ was out of the range 300–350 Mcps nA^{-1} or if the ratio of $^{12}\text{C}_2\text{H}^+/^{12}\text{C}_2^-$ deviated from the range 0.07–0.27 based on measurement results of RMs. Nine OM measurement results out of thirty-one measured points from the Gunflint Formation were outliers based on these criteria. Seven OM measurement results were also excluded because irregular trends were observed in their cycle-by-cycle data (Appendix S7c). Most outlier data have a larger analytical precision than bracketing UWLA-1 measurement results ($\sim 0.6\%$ for $\delta^{15}\text{N}$ results of OM; Appendix S4). Such irregular measurement results could result from inclusions or amorphous carbon phases that have different composition or ionisation efficiency.

The contamination of epoxy was carefully monitored based on the procedures performed by Williford *et al.* (2016). The possible penetration of epoxy into sample pores was assessed using transmitted light microscopy observation. The SIMS pits after measurement were examined by EDS to monitor chlorine, which is a common minor constituent of epoxy (Appendix S8). In addition, the typical yields of $^{12}\text{C}_2^-$ and $^{12}\text{C}^{14}\text{N}^-$ ion on epoxy were ~ 250 Mcps nA^{-1} and ~ 100 Mcps nA^{-1} , which are distinguishable from those of RMs and sample OM. Even in the case that a small amount of epoxy would have contaminated the examined OM, it could be detectable as an irregular cycle-by-cycle trend in each single measurement.

Contamination of carbon and nitrogen components from matrix carbonate is negligible due to low yields of molecular ions. Calcite UWC-3, which is commonly used as a RM for SIMS measurements of $\delta^{13}\text{C}$ in carbonate (e.g., Kozdon *et al.* 2009, Ferry *et al.* 2010, Williford *et al.* 2016), was analysed using the methods of this study. Typical yields were

0.07 Mcps nA^{-1} for $^{12}\text{C}_2^-$ ions and 0.01 Mcps nA^{-1} for $^{12}\text{C}^{14}\text{N}^-$ ions, respectively. Compared with typical ion beam intensities of UWLA-1 anthracite (330 and 17 Mcps nA^{-1} , respectively), contributions of these ions from carbonate are negligible and smaller than the analytical precision. This difference of ionisation efficiency results from differences of chemical bonding of carbon and concentration of nitrogen. Anthracite contains abundant C–C bonds, as both aromatic and saturated and unsaturated hydrocarbons, whereas carbonate contains C–O bonds. This difference makes the ionisation of $^{12}\text{C}_2^-$ ions in anthracite more efficient than in carbonate. The ionisation efficiency of $^{12}\text{C}_2^-$ ions in carbonate is $\sim 4.7 \times 10^3$ times lower than that of anthracite. This further suggests the possibility that the C–C bond in the target material is required for the purpose of $^{12}\text{C}_2^-$ ion intensity measurement by the SIMS. The yields of $^{12}\text{C}^{14}\text{N}^-$ ions on UWC-3 were negligibly smaller than the measurement precision. The origin of nitrogen in UWC-3 is unclear, and several factors such as atmosphere in the analysis chamber, micrometre-scale RM debris or epoxy contaminated during polishing are considered. These differences in ionisation efficiency of $^{12}\text{C}_2^-$ and $^{12}\text{C}^{14}\text{N}^-$ ions suggest that measurement of molecular ions, as demonstrated in this study, will be highly advantageous in studies analysing reduced carbonaceous matter in a carbonate matrix.

Palaeoproterozoic organic matter

A total of twenty-two points were analysed in the Gunflint OM from the carbonate-rich thin section along with bracketing measurements of UWLA-1 (Appendix S9). Data were processed by the following procedure after rejection of outliers based on the RM threshold, defined in the former section. The mean values for $^{12}\text{C}_2^-$, $^{12}\text{C}^{14}\text{N}^-$ yields and $^{12}\text{C}_2\text{H}^+/^{12}\text{C}_2^-$ ratios of the Gunflint Formation OM were 329, 23.4 and 0.24 Mcps nA^{-1} , respectively. After the tailing correction, carbon and nitrogen isotope values were determined by the following equations:

$$\delta^{13}\text{C}_{\text{VPDB}}(\text{sample}) = \left[\frac{(\delta^{13}\text{C}_{\text{Raw}}/10^3 + 1)}{(\text{Bias}(\text{C})_{\text{sample}}/10^3 + 1)} - 1 \right] \times 10^3 \quad (12)$$

$$\delta^{15}\text{N}_{\text{Air}}(\text{sample}) = \left[\frac{(\delta^{15}\text{N}_{\text{Raw}}/10^3 + 1)}{(\text{Bias}(\text{N})_{\text{sample}}/10^3 + 1)} - 1 \right] \times 10^3 \quad (13)$$

where $\delta^{13}\text{C}_{\text{VPDB}}(\text{sample})$ and $\delta^{15}\text{N}_{\text{Air}}(\text{sample})$ are values calculated based on international measurement standards. $\text{Bias}(\text{C})_{\text{sample}}$ was calculated from Equations (7, 8, 10)

(Figure 3a) and $^{12}\text{C}_2\text{H}/^{12}\text{C}_2$ ratios of each measurement spot. $\text{Bias}(\text{N})_{\text{sample}}$ was calculated from the average of Bias (N) of bracketing measurements and Equation (8), respectively. All data are summarised in Table 4. Eight to nine spots of UWLA-1 were measured to bracket every approximately ten measurements of OM samples. Values of $\delta^{13}\text{C}_{\text{VPDB}}(\text{sample})$ and $\delta^{15}\text{N}_{\text{Air}}(\text{sample})$ ranged from -33.8 to -33.3‰ and +4.2 to +5.8‰, respectively.

The $\delta^{15}\text{N}_{\text{Air}}(\text{sample})$ values of UWMA-1 and SH95-S1a, which are from Palaeoproterozoic OM-rich sediments, were $5.9 \pm 0.70\text{‰}$ and $3.1 \pm 0.70\text{‰}$ based on bracketing measurements of UWLA-1 and Equations (12, 13) in session 2 (2s; Table 3). These measurement results are reasonably consistent with bulk data of $\delta^{15}\text{N}$ within analytical precision (Table 1), suggesting that the mass bias calibration of nitrogen based on the bracketing measurements of UWLA-1 in the present study is suitable for analysis of Palaeoproterozoic OM.

This is the first report to obtain $\delta^{15}\text{N}$ values and its low variance within analytical precision in UWMA-1, which is the oldest known anthracite (1850 Ma, Michigamme Fm., USA; Tyler *et al.* 1957), and SH95-S1a, shungite (2100 to 2000 Ma, Karelia, Russia; Buseck *et al.* 1997). Both of these samples have smaller $^{12}\text{C}_2\text{H}/^{12}\text{C}_2$ ratios and higher $^{12}\text{C}_2$ yields than the anthracite RMs, which are Phanerozoic in age (Table 3). These differences imply that the degree of graphitisation of OM and increased C-C bonds in OM yield more efficient generation of $^{12}\text{C}_2$ ions.

The intermediate precision of each bracket was determined by calculating two standard deviations of $\delta^{13}\text{C}_{\text{meas}}$ and $\delta^{15}\text{N}_{\text{meas}}$ mean values on UWLA-1 ($N = 38$). Mean intermediate precisions of UWLA-1 were $\pm 0.16\text{‰}$ for carbon and $\pm 0.56\text{‰}$ for nitrogen, through session 2 (Appendix S4; 2s). The analytical precision of one measurement on each spot was calculated based on two standard deviations of the mean of the twenty cycles that make up a single measurement (we hereafter refer to this analytical precision as the 'internal precision'). However, the internal precision can be influenced by several factors, including not only how heterogeneous the distribution of material or isotope ratios with depth is, but also the change of trajectory of secondary ion beam according to the pit that was sputtered by the primary ion beam. Thus, the internal precision of SIMS measurement does not reflect the true depth heterogeneity. The mean internal precision of UWLA-1 measurements was smaller than the mean intermediate precision of bracketing measurement during sample measurements (Appendix S4). Average internal precision of Gunflint OM was similar ($\pm 0.20\text{‰}$ for $\delta^{13}\text{C}$, $\pm 0.40\text{‰}$ for

$\delta^{15}\text{N}$, 2s) to that of UWLA-1 measurements (Appendix S4). Thus, in the present study, the analytical precision for $\delta^{13}\text{C}_{\text{VPDB}}(\text{sample})$ and $\delta^{15}\text{N}_{\text{Air}}(\text{sample})$ values of each unknown analysis was propagated by intermediate precision of bracketing measurement of UWLA-1 (Table 4).

In summary, the variations in both $\delta^{13}\text{C}_{\text{VPDB}}(\text{sample})$ and $\delta^{15}\text{N}_{\text{Air}}(\text{sample})$ values determined on the OM samples can be explained by the analytical precision of each data. Means of $\delta^{13}\text{C}_{\text{VPDB}}(\text{sample})$ and $\delta^{15}\text{N}_{\text{Air}}(\text{sample})$ values of Gunflint OM were $-33.5 \pm 0.25\text{‰}$ and $+5.2 \pm 0.81\text{‰}$, respectively ($n = 22$, 2s). The bulk $\delta^{13}\text{C}_{\text{VPDB}}$ and $\delta^{15}\text{N}_{\text{Air}}$ values of kerogen, extracted from the same rock sample, were $-32.9 \pm 0.4\text{‰}$ and $+6.9 \pm 0.6\text{‰}$, respectively (Table 1). Thus, the $\delta^{13}\text{C}$ and $\delta^{15}\text{N}$ values of both SIMS and bulk kerogen measurement results are consistent within analytical precision (based on the comparison calculation by Linsinger 2010).

Ishida *et al.* (2012) reported heterogeneous distribution of $\delta^{15}\text{N}$ values in bulk samples of kerogen, chemically isolated by HCl/HF acid treatment, from the same rock as Gunflint sample #0708. In Ishida *et al.* (2012), the $\delta^{15}\text{N}$ values were measured by the stepwise combustion method, which resolves the complex origin of organic $\delta^{15}\text{N}$ values based on the combustion temperatures of each organic component, and it was concluded that the kerogen contains at least two reservoirs with different $\delta^{15}\text{N}$ compositions: $+5.0 \pm 0.6\text{‰}$ and $+7.3 \pm 0.4\text{‰}$. This variation in $\delta^{15}\text{N}$ values was not recognised in the present study, suggesting that such heterogeneous reservoirs might be distributed as a mixture of OM in a smaller scale than the spot size of SIMS measurement, 12 μm .

Contamination of measured OM by ammonium (NH_4^+) is less likely. The substitution of NH_4^+ in sediments is commonly found in phyllosilicates where it substitutes for K^+ (Shen *et al.* 2006). EDS analyses of minor component of OM on each SIMS pit indicated that 0 to 1.4 g/100 g, with mean value of 0.2 g/100 g, of Si or Al was included in examined OM, while K was not detected (Appendix S8). Even in the case where 1.4 g/100 g of clay mineral was included in the OM, the contribution of ammonium would be negligible compared with the nitrogen concentration of the OM. In addition, although the OM was investigated by SEM/EDS and measurement data by SIMS in the present study, evidence of contamination, such as from epoxy, which can be a source of different $\delta^{15}\text{N}$ components, was not identified.

The Michigamme anthracite, which was deposited in the same sedimentary basin (Animikie Basin), but is younger than the Gunflint Formation, has similar $\delta^{13}\text{C}$ and $\delta^{15}\text{N}$ values with a lower variance of nitrogen isotope ratios (Table 3). This difference might be caused by the change of

Table 4. Summary of SIMS measurement results and corrected $\delta^{13}\text{C}_{\text{VPDB}}$ and $\delta^{15}\text{N}_{\text{AIR}}$ values of organic matter from Gunflint sample .0708 measured in session 2. For full data set, see Appendix S4

Sample ID	$\delta^{13}\text{C}_{\text{VPDB}}$ (sample) (‰)	$2s^a$ (‰)	$\delta^{15}\text{N}_{\text{AIR}}$ (sample) (‰)	$2s^a$ (‰)	$\delta^{13}\text{C}_{\text{Raw}}$ (‰)	$2SE^b$ (‰)	$\delta^{15}\text{N}_{\text{Raw}}$ (‰)	$2SE^b$ (‰)	$^{12}\text{C}_2$ yield (Mcps nA^{-1})	$^{12}\text{C}^{14}\text{N}$ yield (Mcps nA^{-1})	$^{12}\text{C}_2\text{H}/$ $^{12}\text{C}_2$	$2SE^b$	$^{12}\text{C}_2\text{H}$ tail ^c (‰)	$^{13}\text{C}^{14}\text{N}$ tail ^d (‰)	Bias (C) (‰)	Bias (N) (‰)
OM18 g3	-33.5	0.16	5.7	0.60	-40.2	0.20	-6.3	0.40	329.9	23.1	0.24	0.13	0.64	0.055	-7.68	-12.0
OM18 g4	-33.4	0.16	5.0	0.60	-40.2	0.20	-7.0	0.50	332.4	23.3	0.24	0.12	0.64	0.055	-7.67	-12.0
OM18 g5	-33.4	0.16	5.5	0.60	-40.2	0.18	-6.5	0.47	321.5	22.4	0.24	0.15	0.65	0.055	-7.70	-12.0
OM18 g6-1	-33.8	0.16	5.1	0.60	-40.2	0.18	-6.9	0.47	327.4	23.4	0.20	0.10	0.54	0.055	-7.14	-12.0
OM18 g6-2	-33.3	0.16	5.0	0.60	-40.1	0.21	-7.0	0.32	322.1	23.0	0.24	0.15	0.65	0.055	-7.71	-12.0
OM18 g7	-33.5	0.16	5.4	0.60	-40.3	0.21	-6.5	0.35	332.9	23.7	0.24	0.12	0.64	0.055	-7.66	-12.0
OM18 g9	-33.6	0.16	5.2	0.60	-40.3	0.18	-6.8	0.40	333.3	23.9	0.24	0.15	0.63	0.055	-7.62	-12.0
OM18 g10-2	-33.4	0.16	4.2	0.60	-40.2	0.20	-7.7	0.50	326.2	23.0	0.24	0.13	0.65	0.055	-7.69	-12.0
OM18 g11	-33.4	0.25	5.8	0.61	-40.2	0.18	-6.2	0.34	328.0	22.9	0.24	0.14	0.65	0.055	-7.67	-12.0
OM05 g1-1	-33.4	0.25	5.2	0.61	-40.2	0.19	-6.8	0.33	328.7	23.3	0.24	0.15	0.65	0.055	-7.68	-12.0
OM05 g1-2	-33.4	0.25	5.4	0.61	-40.1	0.18	-6.7	0.37	332.0	23.6	0.24	0.14	0.64	0.055	-7.65	-12.0
OM05 g2	-33.5	0.25	4.9	0.61	-40.2	0.21	-7.1	0.37	329.9	23.2	0.24	0.14	0.64	0.055	-7.63	-12.0
OM05 g3	-33.7	0.25	5.2	0.61	-40.3	0.24	-6.8	0.43	329.3	23.8	0.23	0.11	0.62	0.055	-7.52	-12.0
OM05 g4	-33.6	0.25	5.0	0.61	-40.3	0.21	-7.0	0.31	330.8	23.2	0.23	0.12	0.63	0.055	-7.58	-12.0
OM05 g5-1	-33.4	0.25	5.7	0.61	-40.2	0.20	-6.4	0.45	328.2	23.0	0.24	0.15	0.65	0.055	-7.66	-12.0
OM05 g5-2	-33.5	0.25	5.5	0.61	-40.3	0.19	-6.5	0.37	326.8	23.2	0.24	0.14	0.65	0.055	-7.67	-12.0
OM05 g6	-33.4	0.25	5.2	0.61	-40.1	0.18	-6.8	0.42	329.9	23.4	0.24	0.14	0.65	0.055	-7.69	-12.0
OM34 g1	-33.3	0.24	4.9	0.51	-40.1	0.20	-7.2	0.44	330.6	23.6	0.24	0.14	0.65	0.055	-7.68	-12.1
OM34 g5	-33.3	0.24	5.1	0.51	-40.1	0.18	-7.1	0.30	328.7	23.3	0.25	0.17	0.66	0.055	-7.75	-12.1
OM40 g1	-33.5	0.24	5.5	0.51	-40.2	0.20	-6.6	0.49	334.0	24.8	0.24	0.15	0.64	0.055	-7.61	-12.1
OM40 g3-1	-33.6	0.24	4.2	0.51	-40.3	0.28	-7.9	0.42	322.0	24.4	0.24	0.13	0.63	0.055	-7.60	-12.1
OM40 g3-2	-33.5	0.24	5.4	0.51	-40.1	0.17	-6.7	0.34	325.0	23.9	0.23	0.15	0.60	0.055	-7.45	-12.1
Mean			5.2		-40.2		-6.8		329	23.4			0.636			
$2s$	0.25		0.81		0.14		0.82		7.2	1.0						

^a Analytical precision propagated by two standard deviation intermediate precision of the bracketing measurement of UWLA-1.

^b $2SE$: two standard deviations of the means of the twenty cycles that make up a single measurement.

^c Amount of tailing correction (in ‰ notation) for the interference of $^{12}\text{C}^{12}\text{CH}$ tail signal to $^{12}\text{C}^{13}\text{C}$.

^d Amount of tailing correction (in ‰ notation) for the interference of $^{13}\text{C}^{14}\text{N}$ tail signal to $^{12}\text{C}^{14}\text{N}$.

sedimentary environment. The Sudbury impact layer corresponds to the top of the Gunflint Formation and separates it from the Michigamme Formations (Addison *et al.* 2005). This event drastically changed ocean chemistry, probably causing a change in the biosphere nitrogen cycle to a simple system from the complex system observed in the Gunflint Formation (Cannon *et al.* 2010).

The 2100 Ma Karelia shungite measurement results have lower variance and show the lowest mean $\delta^{13}\text{C}$ and $\delta^{15}\text{N}$ values (-37.2% and $+3.1\%$, respectively) among the three examined Palaeoproterozoic sedimentary OM samples in this study. The $\delta^{13}\text{C}$ value is lower than typical values that were fractionated by oxygenic photosynthetic bacteria, and is closer to that of methanogens (Schidlowski 1988). The $\delta^{15}\text{N}$ value of shungite is slightly lower than those of other Palaeoproterozoic samples, but is still in the reasonable range of values produced by the biological nitrogen isotope fractionation under an oxic ocean (i.e., Sigman *et al.* 2009).

The mean $\delta^{13}\text{C}_{\text{VPDB}}(\text{sample})$ and $\delta^{15}\text{N}_{\text{Air}}(\text{sample})$ values determined by SIMS *in situ* measurements in three Palaeoproterozoic OM samples are consistent with those determined by bulk gas-source analysis within analytical precision. These $\delta^{15}\text{N}$ values are comparable to those of Archaean kerogen reported by Stüeken *et al.* (2015), and their chronological transition, which may constrain the evolution history of enzymes, such as *nitrogenase*. $\delta^{13}\text{C}$ values also can be used as an indicator to understand the enzymatic metabolic pathway in conjunction with metal elements, which can be an indicator of enzymes (e.g., Schidlowski 1988, Moore *et al.* 2017). The micrometre-scale co-study of $\delta^{13}\text{C}$ and $\delta^{15}\text{N}$ values in OM, in relation to mineral occurrences and element mass fractions, will provide a more detailed metabolic pathway and corresponding environment at that age. To evaluate this possibility, it is necessary to study additional Precambrian samples in association with the bulk rock chemistry and mineralogy. A detailed characterisation of these micrometre-scale geochemical features will allow a more fundamental understanding of low atomic number element isotope geochemistry and may constrain the Precambrian biosphere.

Applications for further study and concluding remarks

In the present study, reference materials and measurement procedures were established for the simultaneous measurement of $\delta^{13}\text{C}$ and $\delta^{15}\text{N}$ from a single $12\ \mu\text{m}$ spot in organic matter by SIMS. Mass bias calibration is required for carbon isotope ratio measurements based on $^{12}\text{C}_2\text{H}^-$ ratios, while mass bias of nitrogen does not require a matrix

correction for variable $^{12}\text{C}_2\text{H}^-$ ratios. Ionisation efficiency of $^{12}\text{C}_2^-$ ions in carbonate is significantly lower than that of reduced organic matter because of the difference in carbon bonding between these materials. Measurement of $^{12}\text{C}_2^-$ ions is highly advantageous for micrometre-scale organic matter in a carbonate matrix.

Analysis of twenty-two OM globules from unmetamorphosed carbonate of the Palaeoproterozoic Gunflint Formation shows homogeneous $\delta^{13}\text{C}_{\text{VPDB}}(\text{sample})$ and $\delta^{15}\text{N}_{\text{Air}}(\text{sample})$ values within analytical precision. These carbon and nitrogen isotope characteristics are consistent with those measured in the Gunflint Formation in previous studies (e.g., Schidlowski 1988, House *et al.* 2000, Poulton *et al.* 2004, Godfrey *et al.* 2013, Williford *et al.* 2013), as well as with biological carbon and nitrogen cycling models in the Gunflint ocean, where oxygenic photosynthetic bacteria lived as primary producers in the shallow ocean (e.g., Ishida *et al.* 2017).

The $\delta^{15}\text{N}$ values found for the 1850 Ma Michigamme anthracite and the 2100 Ma Karelia shungite were $5.9 \pm 0.7\%$ and $3.1 \pm 0.7\%$, respectively ($n = 4$, $2s$). These differences in $\delta^{15}\text{N}$ values and homogeneity among examined Palaeoproterozoic organic matter samples suggest differences of ocean chemistry and microbial activity.

Simultaneous measurement of carbon and nitrogen of OM, such as kerogen, pyrobitumen and microfossil samples found in Precambrian sedimentary rocks, can be made *in situ*, allowing correlations with textures and other geochemistry. The sedimentary structure and occurrence of minerals provide new insight into detailed microbial activity and corresponding sedimentary environments. This work helps to expand the range of analytical tools available for the study of stable isotopes as biosignatures. Furthermore, this quick, precise analytical technique will have applicability to research in modern biological studies such as the following: using $\delta^{13}\text{C}$ and $\delta^{15}\text{N}$ as a proxy of modern or ancient food chains; determining the maturation of coal; fossil-based study of palaeo-ecosystems; and palaeoclimatology targeting organic matter in marine biocarboxates.

Acknowledgements

We are grateful to Noriko Kita for her technical advice of SIMS; Michael J. Spicuzza and Yuki Kunitake who helped to measure bulk carbon and nitrogen isotope ratios of RMs; Brian Hess for his technical contribution of preparing RMs mount; and Bob Dott who introduced us to the Michigamme anthracite that was originally collected by Stanley A. Tyler.

We thank two anonymous reviewers and the editor Thomas Meisel for constructive comments on this work. This research was principally supported by the NASA Astrobiology Institute (NAI-144-PRJ-67ZB). The WiscSIMS laboratory is supported by National Science Foundation (EAR-1355590, -1658823) and the University of Wisconsin-Madison. K.H.W. and M.L.T. acknowledge the support of a grant from the National Aeronautics and Space Administration for work performed at the Jet Propulsion Laboratory, California Institute of Technology.

References

Addison W.D., Brumpton G.R., Vallini D.A., McNaughton N.J., Davis D.W., Kissin S.A., Fralick P.W. and Hammond A.L. (2005)

Discovery of distal ejecta from the 1850 Ma Sudbury impact event. *Geology*, 33, 193–196.

Ader M., Cartigny P., Boudou J., Oh J., Petit E. and Javoy M. (2006)

Nitrogen isotopic evolution of carbonaceous matter during metamorphism: Methodology and preliminary results. *Chemical Geology*, 232, 152–169.

Beaumont V. and Robert F. (1999)

Nitrogen isotope ratios of kerogens in Precambrian cherts: A record of the evolution of atmosphere chemistry? *Precambrian Research*, 96, 63–82.

Bell E.A., Boehnke P., Harrison T.M. and Mao W.L. (2015)

Potentially biogenic carbon preserved in a 4.1 billion-year-old zircon. *Proceedings of the National Academy of Sciences of the United States of America*, 112, 14518–14521.

Buseck P.R., Galdobina L.P., Kovalevski V.V., Rozhkova N.N., Valley J.W. and Zaidenberg A.Z. (1997)

Shungites: The C-rich rocks of Karelia, Russia. *Canadian Mineralogist*, 35, 1363–1378.

Cannon W.F., Schulz K.J., Horton J.W. Jr and Kring D.A. (2010)

The Sudbury impact layer in the Paleoproterozoic iron ranges of northern Michigan, USA. *Geological Society of America Bulletin*, 122, 50–75.

Craig H. (1957)

Isotopic standards for carbon and oxygen and correlation factors for mass-spectrometric analysis of carbon dioxide. *Geochimica et Cosmochimica Acta*, 12, 133–149.

Ferry J.M., Ushikubo T., Kita N.T. and Valley J.W. (2010)

Assessment of grain-scale homogeneity and equilibration of carbon and oxygen isotope compositions of minerals in carbonate-bearing metamorphic rocks by ion microprobe. *Geochimica et Cosmochimica Acta*, 74, 6517–6540.

Fralick P., Davis D.W. and Kissing S.A. (2002)

The age of Gunflint Formation, Ontario, Canada: Single

zircon U-Pb age determinations from reworked volcanic ash. *Canadian Journal of Earth Science*, 39, 1085–1091.

Godfrey L.V., Poulton S.W., Bebout G.E. and Fralick P.W. (2013)

Stability of the nitrogen cycle during development of sulfidic water in the redox-stratified late Paleoproterozoic Ocean. *Geology*, 41, 655–658.

House C.H., Schopf J.W., McKeegan K.D., Coath C.D., Harrison T.M. and Stetter K.O. (2000)

Carbon isotopic composition of individual Precambrian microfossils. *Geology*, 28, 707–710.

Ishida A., Hashizume K. and Kakegawa T. (2012)

Stepwise combustion analyses of distinct nitrogen isotopic compositions on Paleoproterozoic organic matter. *Geochemical Journal*, 46, 249–253.

Ishida A., Hashizume K. and Kakegawa T. (2017)

Microbial nitrogen cycle enhanced by continental input recorded in the Gunflint Formation. *Geochemical Perspective Letters*, 4, 13–17.

Ito M., Uesugi M., Naraoka H., Yabuta H., Kitajima F., Mita M., Takano Y., Karouji Y., Yada T., Ishibashi Y., Okada T. and Abe M. (2014)

H, C, and N isotopic compositions of Hayabusa category 3 organic samples. *Earth, Planets and Space*, 66, 1–8.

Junk G. and Svec H. (1958)

The absolute abundance of the nitrogen isotopes in the atmosphere and compressed gas from various sources. *Geochimica et Cosmochimica Acta*, 14, 234–243.

Kita N.T., Ushikubo T., Fu B. and Valley J.W. (2009)

High precision SIMS oxygen isotope analysis and the effect of sample topography. *Chemical Geology*, 264, 43–57.

Kita N.T., Huberty J.M., Kozdon R., Beard B.L. and Valley J.W. (2011)

High precision SIMS oxygen, sulfur and iron stable isotope analyses of geological materials: Accuracy, surface topography and crystal orientation. *SIMS XVII Proceedings, Surface and Interface Analysis*, 43, 427–431.

Kozdon R., Ushikubo T., Kita N.T., Spicuzza M. and Valley J.W. (2009)

Intratest oxygen isotope variability in planktonic foraminifera: New insights from *in situ* measurements by ion microprobe. *Chemical Geology*, 258, 327–337.

Linsinger T. (2010)

Comparison of a measurement result with the certified value. Application Note 1 EC-JRS IRMM. European Commission-Joint Research Centre Institute for Reference Materials and Measurements (Geel, Belgium), 2pp.



references

- Mills J.S., White R. and Gough L.J. (1984)**
The chemical composition of Baltic amber. *Chemical Geology*, 47, 15–39.
- Moore E.K., Jelen B.I., Giovannelli D., Raanan H. and Falkowski P.G. (2017)**
Metal availability and the expanding network of microbial metabolisms in the Archaean eon. *Nature Geoscience*, 10, 629–636.
- Morag N., Williford K.H., Kitajima K., Philippot P., Van Kranendonk M.J., Lepot K., Thomazo C. and Valley J.W. (2016)**
Microstructure-specific carbon isotopic signatures of organic matter from ~3.5 Ga cherts of the Pilbara Craton support a biological origin. *Precambrian Research*, 275, 429–449.
- Nomaki H., Bernhard J.M., Ishida A., Tsuchiya M., Uematsu K., Tame A., Kitahashi T., Takahata N., Sano Y. and Toyofuku T. (2016)**
Intracellular isotope localization in *Ammonia* sp. (Foraminifera) of oxygen-depleted environments: Results of nitrate and sulfate labelling experiments. *Frontiers in Microbiology*, 7, 163.
- Pinti D.L. and Hashizume K. (2011)**
Early life record from nitrogen isotopes. In: Golding S. and Glikson M. (eds), *Earliest life on Earth: Habitats, environments and methods of detection*. Springer (Dordrecht, The Netherlands), 183–205.
- Poulton S.W., Fralick P.W. and Canfield D.E. (2004)**
The transition to a sulphidic ocean, ~1.84 billion years ago. *Nature*, 431, 173–177.
- Sangely L., Chaussidon M., Michels R. and Huault W. (2005)**
Microanalysis of carbon isotope composition in organic matter by secondary ion mass spectrometry. *Chemical Geology*, 223, 179–195.
- Schidlowski M. (1988)**
A 3,800-million-year isotopic record of life from carbon in sedimentary rocks. *Nature*, 333, 313–318.
- Schimmelmann A. and Lis G.P. (2010)**
Nitrogen isotopic exchange during maturation of organic matter. *Organic Geochemistry*, 41, 63–70.
- Shen Y., Pinti D.L. and Hashizume K. (2006)**
Biogeochemical cycles of sulfur and nitrogen in the Archaean ocean and atmosphere. In: Benn K., Mareschal J.C. and Condie K. (eds), *Archaean geodynamics and environments*, Geophysical Monograph Series, 164, 305–320.
- Sigman D.M., Karsh K.L. and Casciotti K.L. (2009)**
Ocean process tracers: Nitrogen isotopes in the ocean. *Encyclopaedia of ocean science* (2nd edition). Elsevier (Amsterdam), 4138–4153.
- Smart K.A., Tappe S., Stern R.A., Webb S.J. and Ashwal L.D. (2016)**
Early Archaean tectonics and mantle redox recorded in Witwatersrand diamonds. *Nature Geoscience*, 9, 255–259.
- Stüeken E.E., Buick R., Guy B.M. and Koehler M.C. (2015)**
Isotopic evidence for biological nitrogen fixation by molybdenum-nitrogenase from 3.2 Gyr. *Nature*, 520, 666–674.
- Stüeken E.E., Zaloumis J., Meixnerová J. and Buick R. (2017)**
Differential metamorphic effects on nitrogen isotopes in kerogen extracts and bulk rocks. *Geochimica et Cosmochimica Acta*, 217, 80–94.
- Thomazo C., Pinti D.L., Busigny V., Ader M., Hashizume K. and Philippot P. (2009)**
Biological activity and the Earth's surface evolution: Insights from carbon, sulfur, nitrogen and iron stable isotopes in the rock record. *Comptes Rendus Palevol*, 8, 665–678.
- Tyler S.A., Barghoom E.S. and Barrett L.P. (1957)**
Anthracitic coal from Precambrian Upper Huronian Black Shale of the Iron River District, Northern Michigan. *Geological Society of America Bulletin*, 68, 1293–1304.
- Ushikubo T., Williford K.H., Farquhar J., Johnston D.T., Van Kranendonk M.J. and Valley J.W. (2014)**
Development of *in situ* sulfur four-isotope analysis with multiple Faraday cup detectors by SIMS and application to pyrite grains in a Paleoproterozoic glaciogenic sandstone. *Chemical Geology*, 383, 86–99.
- Valley J.W. and Kita N.T. (2009)**
In situ oxygen isotope geochemistry by ion microprobe. In: Fayek M. (ed.), *Secondary ion mass spectrometry in the Earth sciences*, Mineralogical Association of Canada Short Course, 41, 19–63.
- Wacey D., McLoughlin N., Kilburn M.R., Saunders M., Cliff J.B., Kong C., Barley M.E. and Brasier M.D. (2013)**
Nanoscale analysis of pyritized microfossils reveals differential heterotrophic consumption in the ~1.9-Ga Gunflint chert. *Proceedings of the National Academy of Sciences of the United States of America*, 110, 8020–8024.
- Wacey D., Saunders M., Kong C. and Kilburn M.R. (2016)**
A new occurrence of ambient inclusion trails from the ~1900-million-year-old Gunflint Formation, Ontario: Nanocharacterization and testing of potential formation mechanisms. *Geobiology*, 14, 440–456.
- Williford K.H., Ushikubo T., Schopf J.W., Lepot K., Kitajima K. and Valley J.W. (2013)**
Preservation and detection of microstructural and taxonomic correlations in the carbon isotopic compositions of individual Precambrian microfossils. *Geochimica et Cosmochimica Acta*, 104, 165–182.
- Williford K.H., Ushikubo T., Lepot K., Kitajima K., Hallmann C., Spicuzza M.J., Kozdon R., Eigenbrode J.L., Summons R.E. and Valley J.W. (2016)**
Carbon and sulfur isotopic signatures of ancient life and environment at the microbial scale: Neoproterozoic shales and carbonates. *Geobiology*, 14, 105–128.

Supporting information

The following supporting information may be found in the online version of this article:

Appendix S1. Schematic of the IMS 1280 multi-collector system block.

Appendix S2. Element mass fractions of reference materials and organic matter of the Gunflint Formation.

Appendix S3. Backscattered electron images of SIMS pits of examined organic matter of Gunflint sample #0708.

Appendix S4. All SIMS analytical data from sessions 1 and 2.

Appendix S5. Time sequence of ninety-five measurements of nitrogen isotope ratios of reference materials in session 1.

Appendix S6. Correlation diagrams of reference materials measured in session 2.

Appendix S7. Comparison of the cycle-by-cycle trends of representative samples.

Appendix S8. Results of EDS analysis of minor elements measured adjacent to SIMS pits of examined organic matter, reference materials and epoxy.

Appendix S9. Time sequences of $\delta^{13}\text{C}_{\text{Raw}}$ and $\delta^{15}\text{N}_{\text{Raw}}$ values during measurements of organic matter (Gunflint #0708) and reference material UWLA-1 (anthracite).

This material is available as part of the online article from: <http://onlinelibrary.wiley.com/doi/10.1111/ggr.12209/abstract> (This link will take you to the article abstract).